Internal Energy Distribution in Electrospray Ionization from the Multiple-Collision Model: The case of a Thermal-Like Distribution

David Rondeau,[a,b] László Drahos[c] and Károly Vékey[c]

a. Institut d'Electronique et de Télécommunication de Rennes (IETR UMR CNRS 6164), Université de Rennes 1, Campus de Beaulieu, 263 Avenue du General Leclerc, 35042 Rennes Cedex.
b. Université de Bretagne Occidentale, Département de Chimie, 6 avenue le Gorgeu, 29238 Brest Cedex 03.
c. Mass Spectrometry Department, Center of the Hungarian Academy of Sciences, Puszteszeri ut 59–67, H-1025 Budapest, Hungary.

ABSTRACT

In the presented study, the ion survival yields of the theoretical mass spectra simulated by the MassKinetic software are fitted with the experimental ion survival yield of substituted benzylpyridinium cations reported in a precedent paper (*J. Mass Spectrom.* **1999**, *34*, 1373-1379). A partially elastic multiple collision model is considered for describing the ion behaviour into the desolation area of the ESI source. The adjusting parameters are not the shape and the position of the $P(E_{int})$ curve but rather parameters related to the source acting, such as the pressure and the kinetic energy of ions entering the desolvation zone. In the case of a PE SCIEX ESI source interfaced with a quadrupole mass spectrometer, the energy uptake can then be well-defined by considering the case of a thermal-like distribution an average number of "effective" collisions of 29. From this model, it's possible to correlate the voltage values applied on the orifice of the desolvation area to initial kinetic energy of ions entering into the collision zone of the ESI source. In the present case, these theoretical initial kinetic energy values range from 5.5 to 9 eV and the results of calculations shown also that the mean internal energy $<E_{int}>$ increases linearly with the orifice voltage. This modelling allows defining the internal energy distribution of ions in different part of the ESI source. The activation conditions occurring into the studied ESI source can be compared to a warm-up of ions. Indeed, the internal energy distributions resemble to thermal distribution of ions having a "characteristic temperature" (T_{char}) parameter between 1020 to 1550 K. In addition, this study evidences a linear correlation between $<E_{int}>$ and T_{char}. The slope value of this curve can be related to a calorimetric parameter such as the heat capacity of the activated substituted benzytlpyridinium cations.

INTRODUCTION

Evaluate the amount of internal energy transferred in a gaseous ion during the ionization step is of a fundamental importance in mass spectrometry.[1,2] The internal energy effects are related to the extent of ion fragmentation inducing the appearance of the mass spectrum.[3] It's thus important to elaborate of method able for modelling the internal energy distribution $P(E_{int})$ of the ions produced in the ionization source of a mass spectrometer. This is particularly relevant in the case of the electrospray ionisation (ESI) method that is one the so-called soft ionization sources the most uses in mass spectrometry.[4,5] In ESI, the sample is initially ionized in solution and ions are generated in the gas phase by ion evaporation or Coulombic fission occurring from highly charged solvent droplets.[6,7,8,9] The ionic species emitted into the gas phase can remain solvated as they enter the ion sampling region that separate the atmospheric pressure of the analyser vacuum and even, they can form solvent adducts into this region.[10,11,12,13] This zone delimited by an orifice/skimmer or capillary/skimmer arrangement, is maintained at relatively low pressures (typically of the torr order) and contains remaining gas molecules that allow to an additional supra-thermal-like desolvation step.[5,14] This one is helped by application of a potential difference applied between the items delimiting this zone.[15] According to the increasing of the electric field strengths, the so-called in-source collision induced dissociation (CID) process leads either to remove the last solvent molecules or to fragment the desolvated ions.[16,17] This step is known to be involved in the build-up of the internal energy (E_{int}) of the ions produced in an ESI source.[18,19] The modelling of this collision energy uptake by the ions has been the subject of several studies in order to better rationalize the internal energy distribution of ions produced in an ESI source.

De Pauw and coworkers have proposed a method referenced as the "survival yield" (SY) method, for evaluating the ion internal energy distribution of the electrosprayed ions.[20] This method is based on the relationship between the degree of fragmentation of "thermometer ions" and their amount of internal energy.[21] The SY method used in most cases, different substituted benzylpyridinium cations by considering a simple fragmentation scheme that leads to the loss of neutral pyridine and the formation a substituted benzyl cation.[22] Note that even though more recently the possibility to take into account some alternative fragmentation channels has been proposed in the literature, this is the occurrence of a fragmentation by a direct cleavage of the central C-N bond that is currently considered in first approximation in the SY method.[23,24,25,26,27] The survival yield SY of a parent ion M^+ is related to the abundance of this parent ion $I_M{}^+$ and the fragment ions $I_F{}^+$ measured from the recorded ion source mass spectra such as:

$$SY = \frac{I_{P^+}}{\left(I_{P^+} + \sum_{F^+=1}^{n} I_{F^+} \right)} \quad (1)$$

The survival yield of equation 1, represents the fraction of ions having internal energy less than the appearance energetic threshold E_{thr} of the fragment ions. The value of E_{thr} is obtained from the kinetic shift (E_{ks}) that represents the excess of energy by comparison to the critical energy of the reaction E_0, necessary to fragment the ions at observable rates,[2] such as:

$$E_{ks} = E_{thr} - E_0 \quad (2)$$

It has been shown that E_{ks} can be calculated using the Rice-Ramsperger-Kassel-Marcus (RRKM) theory as a function of the time of flight of the ions after their activation.[28,29,30] In practice, the experimental survival yield (SY_{Exp}) of each thermometer ion is plotted as a function of either their E_{thr} or E_0 values. The weakest ions have then a low survival yield whereas the ions characterized by a high value of E_{thr} are expected to remain intact as they cross the collision zone. If the curve that connects the different SY_{Exp} values a function of their known E_{thr} values allows to fit the data with a single, symmetrical sigmoid function, this one can be considered as an integration of a distribution of ions having energies between E_{int} and E_{int} + d(E_{int}) in limits such as E_{int} = 0 and E_{int} = E_{thr}. Then its derivative leads to express a Gaussian like internal energy distribution $P(E_{int})$ of the electrosprayed ions. The SY_{Exp} measurements have been performed from several ESI sources interfaced with different analyzers and for different experimental conditions such as the voltages applied on the items of the desolvation zone, the source temperature or the nature of the desolvation gaz.[21,31,32,33,34,35] The SY experimental measurements were also combined with the software of Drahos and Vékey that can model the ion behaviour into a designed mass spectrometer by considering namely the ion internal energy distribution among others molecular parameters.[36] In most cases, the theoretical survival yields (SY_{Theo}'s) calculated with MassKinetics are fitted with the measured SY_{Exp}'s by using a model of internal energy distribution $P(E_{int})$ of activated ions as adjusting parameter.[37,38] A slow heating model was retained for describing the internal energy uptake by the ions. As a result, the internal energy distributions $P(E_{int})$ of the activated ions was based on a "thermal-like" Boltzmann distribution related to a simple parameter called the "characteristic temperature" (T_{char}).[32,39,40] This assertion appeared in consistency with the fact that these approximated thermal energy distributions resemble to an internal energy distribution calculated under multiple collision conditions, typically 20 to 40 collisions.[37] More recently it was shown that the internal energy distribution obtained from

ESI source interfaced with a sector mass spectrometer cannot be compared to a "thermal-like" Boltzmann distribution.[35] Such a $P(E_{int})$ was experimentally obtained from the derivative of a sigmoid curve connecting the experimental survival yields (SY_{Exp}) plotted as a function of the thermometer ion E_{thr}. The shape of this distribution was much narrower than a thermal distribution, but was in agreement with the model of a $P(E_{int})$ chosen for obtaining a good fit between the SY_{Theo}'s calculated by MassKinetics and the measured SY_{Exp}'s.

For simulating the multi-collisional heating process occurring within the so-called orifice/skimmer region, Hoxha *et al* have performed calculations ion trajectory using the SIMION program.[41] The adopted statistical model took into account both activation and deactivation processes upon multiple collisions by supposing that the energy is randomly redistributed between the ion and the target gas at each collision. The authors concluded on the fact that 90 % of the internal energy uptake by the ion occurs very close to the skimmer where the ions are subjected to a strong acceleration. This was in agreement with the works of Schneider *et al*.[42] They have developed a semi-quantitative model showing that the small number of high-energy collisions occurring in front of the skimmer is equally effective for the uptake of ion internal energy than a large number of low-energy collisions occurring in the first millimetres of the desolvation region of an ESI source.

Two different approaches can then be considered for evaluating the ion internal energy distributions in an ESI source. The first approach tends to test an internal energy distribution that allows to the best fit between the SY_{Exp}'s and the SY_{Theo}'s. The second approach attempts to simulate the collision events in order to obtain internal energy distributions that are comparable to those evaluated by the SY method.

For the present study we have simulated the behaviour of thermometer ions that cross the desolvation region of an ESI source by using the partially elastic multiple collisions model in order to calculate SY_{Theo}'s values equal to the SY_{Exp}'s measurements available in literature. The experimental data were taken from results obtained with the ESI source of a PE SCIEX API 165 simple quadrupole mass spectrometer.[32] The adjusting parameters used in the model for fitting the experimental data with the calculation results were the pressure of the desolvation area and the initial kinetic energy of the colliding ions. Using the MassKinetics software, the internal energy distributions $P(E_{int})$ of the ion population crossing the collision zone can be then evaluated . Behind the description of the real process occurring into the ESI source, the $P(E_{int})$ of the ions activated by the collision cascade event were compared with "thermal-like" Boltzmann distributions usually calculated from a vibration frequency and the "characteristic temperature" (T_{char}) parameter.

EXPERIMENTAL SECTION

Mass spectrometry and samples

The present work is based on experimental results proposed in the literature by Drahos and co-workers. In their publication, the authors mentioned that the electrospray analyses of the samples were performed on a PE SCIEX API 165 quadrupole mass spectrometer Perkin-Elmer SCIEX (Toronto, Canada) using nitrogen as the nebulizing gas.[32] The experimental conditions interesting the present theoretical study are the following: the voltage on the focusing ring was fixed at 20 V and the orifice voltage (OR voltage) was varied between 0 and 60 V. The voltage on the focusing ring was fixed at 20 V and the voltages of other lenses were optimized for highest sensitivity. The source temperature was set at 180°C. The instrument and ESI source were at room temperature. The four substituted benzylpyridinium cations considered for the present study are regrouped in Table 1.

Structure	Compound name [Abbreviation]	E_0 in eV (*m/z*)
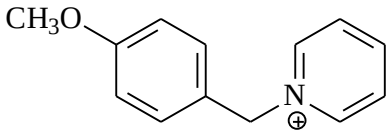	*N*-(4-methoxybenzyl)pyridinium [*p*-CH_3O]	1.76 (200)
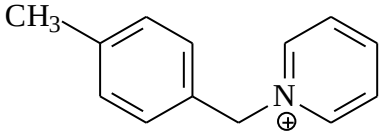	*N*-(4-methylbenzyl)pyridinium [*p*-CH_3]	2.19 (184)
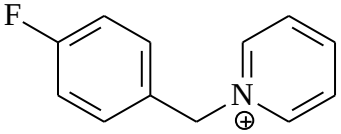	*N*-(4-fluorobenzyl)pyridinium [*p*-F]	2.34 (188)
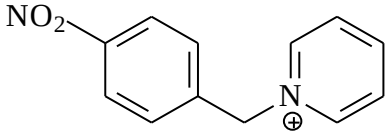	*N*-(4-nitrobenzyl)pyridinium [*p*-NO_2]	2.83 (215)

Table 1: Structure, name, abbreviation (*m/z* ratio) and direct cleavage critical energy E_0 of the substituted benzylpyridinium cations obtained by quantum chemical calculations (see reference [35])

The experimental survival yield (SY_{Exp}) results obtained by Drahos *et al* during their works are regrouped in Table 2 as function of the orifice voltage (OV) value as mentioned in the related publication.[32]

Compound	Experimental Survival Yields (SY_{Exp}'s)				
	10 V	20 V	30 V	40 V	50 V
p-CH_3O	0.68	0.55	0.34	0.17	0.05
p-CH_3	0.97	0.93	0.77	0.53	0.30
p-F	0.99	0.97	0.84	0.61	0.37
p-NO_2	1	1	0.99	0.92	0.81

Table 2: Experimental survival yields of four substituted benzylpyridinium cations measured in the PE SCIEX API 165 quadrupole mass spectrometer as a function of the orifice (OR) voltage value (data from reference [32])

Theoretical modelling of mass spectra

The theoretical survival yield (SY_{Theo}) of each substituted benzylpyridinium cations were calculated using the MassKinetics Scientific (Ver. 1.9) software, available at http://www.chemres.hu/ms/masskinetics.[36] MassKinetics is a general framework for modeling mass spectrometric processes. It combines modeling reaction rates, energy exchanges and product ion abundances as the ions move through various parts of a mass spectrometer. In MassKinetics, the ions are characterized by their internal and kinetic energies, which define the 'state' of a given ion. Essential features of the MassKinetics model are the use of internal and kinetic energy distribution functions together with the probabilities to describe transition between different states. The kinetic and internal energies of the ions in the gas phase may change due to (*i*) acceleration in electromagnetic fields, (*ii*) radiative energy exchange (photon-absorption and emission), (*iii*) collisional energy exchange and (*iv*) energy partitioning in chemical reactions, which are all taken into account.

The fragmentation rate constant ($k^{i,j}(E_{int})$) of a substituted benzylpyridinium cation *i* leading to a substituted benzylium fragment ion *j* at a given internal energy (E_{int}) can be calculated with MassKinetics *via* the transition state theory (TST) in its RRKM formulation such as:

$$k^{i,j}(E_{int}) = \frac{\sigma}{h}\frac{N^{\ddagger}(E_{int} - E_0)}{\rho(E_{int})} \quad (3)$$

In this equation, σ is the reaction degeneracy, h is the Planck's constant, E_0 is the reaction critical energy, $N^{\ddagger}(E_{int}\text{-}E_0)$ is the transition state sum of states from 0 to $E_{int}\text{-}E_0$ and $\rho(E_{int})$ is the density of states at an energy level equal to E_{int}. [43,44,45] For this study, the considered E_0 values are those calculated in a precedent work from quantum chemical calculation using the QCISD//MP2 methodology.[35] These values are reported in Table 1 for the four substituted benzylpyridinium cations considered in the present study. In order to express $\rho(E_{int})$ for any substituted benzylpyridinium cation, the frequency model of the ground state was also obtained from the vibration frequency values calculated at the QCISD//MP2 levels of theory.[35] The evaluation of the vibration frequencies of the activated complex that induce the magnitude of the sum of state $N^{\ddagger}(E_{int}\text{-}E_0)$ was performed by considering a fragmentation of the benzylpyridinium ions that proceeds via a "loose" complex. The later corresponds to a direct cleavage due to a stretching of the C-N bond along the reaction coordinate. In this context, MassKinetics can provide a convenient way to simulating such a transition state by modifying the frequency model of the *p*-CH_3 ground state by removing the frequency corresponding to the elongation of the C-N bond (1200 cm^{-1}) and by scaling five other frequencies allowing to obtained a 10^{14} value of the Arrhenius pre-exponential-like factor (A_{PE}).[35,46,47,48,49] Note that the harmonic oscillator model was applied with internal rotations approximated by low frequency vibrations either for the reactant and the transition state frequency model.

The MS experimental sequence fixed for modelling the ion behaviour in the PE SCIEX API 165 quadrupole mass spectrometer was: (i) ion formation without any internal energy deposited during this process; (ii) ion flight trough a collision zone of 0.013 m length where a 4 V potential difference (ΔV) is applied leading to an ion residence time residence of the microsecond order (iii) electrostatic acceleration under a 10 V potential difference with a 0.21 m flight length and (iv) ion selection following by detection (from the acceleration lens to the detector) with a 0.2 m flight length. The initial internal energy distribution ($P(E_{int})$) of ions prior their collisional activation is a thermal energy distribution at 353 K. The initial kinetic energy ($E_{init,kin}$) of the ions that enter the collision zone is one of the two adjusting parameter chosen for this study. The evolution of its magnitude must be related to the modifications of the voltage values of the orifice of the ESI source used in the publication cited above (see Table 2). The pressure of the target gas (P_G) in the collision zone was the other adjusting parameter in the present study.

Partially elastic multiple collision model

With MassKinetics, the ion abundances and the ion theoretical survival yields can be calculated accurately by following as a function of time, the probability of an ion *i* to be in a given state characterized by a pair of values of internal and kinetic energies noted (E_{int}, E_{kin}).[36] In a multiple collision model where the radiative energy exchange process can be rule out, due to the short residence time of ion into the used mass spectrometer, this probability decreases due either to the fragmentation reaction experienced by the ion and to the collisional activation events.[50] In our case, the later have been modelised by considering the internal energy transfer (IET) function under a simple collision (SC) process for an ion *i* ($P^{IET,SC}$) adapted from the equation of Muntain and Armentrout.[51] The analytical form of this function includes the evaluation of the center of mass energy (E_{com}) such as: $E_{com} = E_{kin} \cdot \frac{m_G}{m_i + m_G}$ (4) where E_{kin} is the kinetic energy of the colliding ion, m_G = 28 u is the mass of nitrogen used as target gaz and m_i, is the mass of the substituted benzylpyridinium cation. The $P^{IET,SC}$ function was evaluated through the partially elastic collision model considering that only a fraction η = 0,128 of E_{com} is converted into internal energy.[52,53] For the multiple collision model, the function $P^{IET,SC}$ must be multiplied by the ion collision frequency (ω_i) that is calculated from: $\omega_i = \sigma_i \left(\sqrt{2E_{kin}/m_i}\right) \frac{P_G}{k_B T_G}$ (5). In equation (5), σ_i is the ion collision cross section, P_G is the collision gas pressure, T_G is the gas temperature related to the temperature of the mass spectrometer and $v_{i,G}$ is the relative velocity of the two collision partners. For this study, P_G was considered as an adjusting parameter, σ_i, = 30 Å² (value considered from literature data) and T_G = 450 K. The later value is a mean temperature that we consider to be representative to the temperatures set for the different in-source CID experiments. In this equation, the target gas is regarded as stationary towards the colliding ion. The translational energy loss during a simple collisional process induces the change in kinetic energy (E_{kin}) for the following collision event. The resulting translation energy loss will induce a modification of the ion collision energy (E'_{kin}) available for a further process such as: $E'_{kin} = E_{kin} - TEL^{PEL}$ (6). In this expression, TEL^{PEL} is the translation energy loss in the partially elastic collisions model. This is a function of E_{com} such as: $TEL^{PEL} = -E_{com} \frac{2m_i + m_G}{m_i + m_G}$ (7) where TEL^{PEL} must be regarded as the kinetic energy (KET)

state transfer probability function from E_{kin} to $E_{kin}^{'}$ in a single collision process $P_i^{KET,SC}\left(E_{kin}^{'}, E_{kin}\right)$.

RESULTS AND DISCUSSION

From the data of Table 2, it appears that an orifice voltage value of 40 V allows to obtain experimental measurements that encompass the widest range of SY_{Exp}'s values, *i.e.* from 0.17 to 0.92. With MassKinetics, several theoretical survival yields (SY_{Theo}'s) have been calculated for the four substituted benzylpyridinium cations and with the two adjusting parameters (E_{kin} and P_G) selected for the theoretical modelling (see Experimental section). The $E_{init,kin}$ and P_G values that lead to the best fit between the SY_{Theo}'s and the SY_{Exp}'s are regrouped in Table 3.

Thermometer ion	**SY_{Theo}**			
	7 eV [a]	8 eV [a]	8 eV [a]	9 eV [a]
	37 Pa [b]	35 Pa [b]	30 Pa [b]	30 Pa [b]
p-CH_3O (E_0 = 1.76 eV)	0.25	0.15	0.29	0.15
p-CH_3 (E_0 = 2.19 eV)	0.67	0.49	0.68	0.48
p-F (E_0 = 2.34 eV)	0.78	0.63	0.79	0.61
p-NO_2 (E_0 = 2.83 eV)	0.99	0.95	0.98	0.94
Calculated Average Number of Collisions	30.7	31.1	26.6	28.2

Table 3: Theoretical survival yields (SY_{Theo}) calculated with MassKinetics as a function of a) the initial kinetic energy ($E_{init,kin}$) of the colliding ions and b) the pressure value of the collision area (P_G). Note that the E_0 values are considered from the dissociation critical energy of Table 1.

The set of values regrouped in Table 3, illustrate the fact that the partially elastic multiple collision model considered for the modelling, can account for the behaviour of thermometer ions crossing the studied ESI source. Indeed, for a same pressure value, *e.g.* P_G = 30 Pa, the increasing in initial kinetic energy of the colliding ions from 8 to 9 eV, leads to a decreasing of all the SY_{Theo}'s. This is due to a greater conversion of $E_{init,kin}$ to the center of mass energy during each collision with the target gas (see equation 4). The decreasing in SY_{Theo} appears greater in the range of low E_0 values (1.76 and 2.19 eV) than for the higher values. This

behaviour is due to the evolution of the magnitude of the fragmentation constant rate $k^{i,j}(E_{int})$ as a function of the density of states in the (E_{int} - E_0) energy ranges (see equation 3). In addition, if the increasing in $E_{init,kin}$ from 8 to 9 eV induces an increasing of ion velocity in the laboratory frame, this change leads also to lower the mean free path of ions in the gas frame. In such a case, the ions undergo more collisions with the background gas. This trend is evidenced by MassKinetics calculations since the average number of collisions is greater at 9 eV than at 8 eV for a same pressure value. The comparison of the SY_{Theo}'s obtained for E_{kin}, = 8 eV and P_G = 35 Pa with the values calculated for $E_{init,kin}$ = 9 eV and P_G = 30 Pa show also that the effect due to the decreasing in E_{kin} could be compensate for by an increasing in P_G. This is in agreement with the fact that the collision frequencies ω_i (see equation 5) must be increased if each collisional event is less energetic. One can argue that these two pairs of values are also the closest to the experimental survival yields measured at a 40 V orifice voltage (see Table 2). However in the case of the present simulation, the value P_G = 35 Pa is the only one that allows to obtained a good fitting between the SY_{Theo} values and the SY_{Exp} data, and this whatever the orifice voltage value applied on the orifice of the PE SCIEX ESI source. This trend is evidenced in Figure 1. This one regroups the curves connecting the theoretical survival yields calculated for different E_0 values and by taking into account the vibration frequencies of the *N*-(4-methylbenzyl)pyridinium cation (*p*-CH_3) as frequency file model for all thermometer ion. In Figure 1, the initial kinetic energy (E_{kin}) values of the colliding ions are the only fitting parameter for adjusting the SY_{Theo} *vs.* E_0 curves with the different SY_{Exp}'s reported in Table 2. One will remark that the different curves of Figure 1 connect all the experimental data.

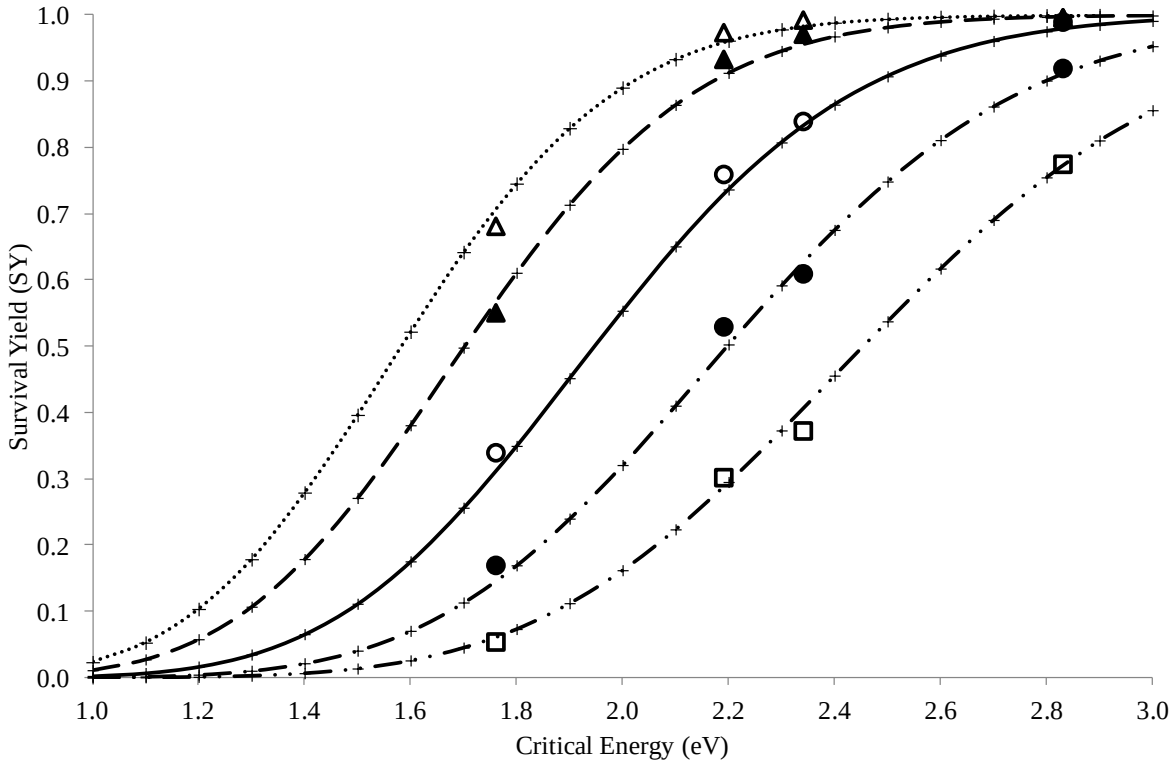

Figure 1: Curves connecting the theoretical survival yields calculated for different values of reaction critical energy (E_0). The different curves of the figure connect the theoretical ion survival yields (+) obtained from the MassKinetics modelling where $E_{\text{init,kin}}$ = 5,5 eV (• •), $E_{\text{init,kin}}$ = 6 eV (— —), $E_{\text{init,kin}}$ = 7 eV (——), $E_{\text{init,kin}}$ = 8 eV (—•—) and $E_{\text{init,kin}}$ = 9 eV (—••—). All calculations were done by considering a 35 Pa pressure of nitrogen in the desolvation zone considered as a collision region. The SY_{Exp} values of the four substituted benzylpyridinium cations (see Table 2) are also plotted as a function of the E_0 values reported in Table 1 by considering the experimental measurements performed at: OR = 10 V (△), OR = 20 V (▲), OR = 30 V (○), OR = 40 V (●) and OR = 50 V (□).

In mildest desolvation conditions represented by the dotted and dashed line in Figure 1 (SY_{Exp}'s at OR = 10 and 20 V), the overall population of *p*-NO_2 cations remains intact. By contrast, almost half of the population of the *p*-CH_3O has not survived. This behaviour experimentally evidenced is in agreement with the calculations performed with $E_{\text{init,kin}}$ = 5.5 and 6 eV (dotted and dashed lines in Figure 1). For these kinetic energy values, the calculated average number of collision is only of 25.8 at $E_{\text{init,kin}}$ = 5.5 eV and 26.9 at $E_{\text{init,kin}}$ = 6 eV. But, the few collisions that occur in the desolvation area are sufficiently reactive for inducing the decay of the weakest ions (E_0 < 2 eV). For more energetic desolvation conditions (dotted-dashed and the dotted-dotted-dashed lines in Figure 1), all the ions dissociate whatever their

fragmentation critical energy and all the more that the average number of collisions is increased until 33 for $E_{init,kin}$ = 9 eV. The theoretical results are in agreement with the SY_{Exp}'s measured at OR = 50 V (see Figure 1). By considering an intermediate kinetic energy value of 7 eV, the average number of collisions able to predict the ion behaviour in the API 165 ESI source can be retained as being of 29 collisions. The average number of collisions that is calculated for our study can be considered as relatively low by comparison to the values available in literature. With their collision dynamics model, Schneider *et al* have calculated a number of collisions greater than 2000 for predicting the E_{com} to E_{int} conversion as a function of the orifice voltage value of the single quadrupole ion spray Sciex mass spectrometer.[42] However, they also proposed that in a ~ 2 mm length area, the hundreds of low-energy collisions that occur in the first 80 μm of the region impart almost the same amount of internal energy as in the ten last collisions occurring 80 µm just before the skimmer. The average number of collisions mentioned in the present study is in agreement with the one proposed by Naban-Maillet et al and must be rather regarded as a set of "effective" collisions.[37] The low "effective" collision frequency highlighted in this paper can account for the significant survival yield measured for the weakest thermometer ions as the *p*-OCH_3 at a 50 V value of the orifice, *i.e.* at $E_{init,kin}$ = 9 eV (see Figure 1). This illustrates that even though the appearance threshold energy is largely reached at such collision energy, a significant proportion of the *p*-OCH_3 ions do no undergo collisions, and thus survives during the crossing of the desolvation region.

The internal energy distributions $P(E_{int})$ of the ion population crossing the different parts of the mass spectrometer can be evaluated by MassKinetics. In order to account for the real physical process characterizing the ion behaviour into the desolvation region, this modelling have to consider that the activation and dissociation of the species occur in parallel with rates that can be on the same order. In this study, the ion internal energy distributions have been calculated for different distances of the ion path into the designed mass spectrometer, *e.g.* by dividing the desolvation area into three equal parts and by delimiting the mass spectrometer by the ion guide and the quadrupole analyzer. The different internal energy distributions the calculated are shown in Figure 2.

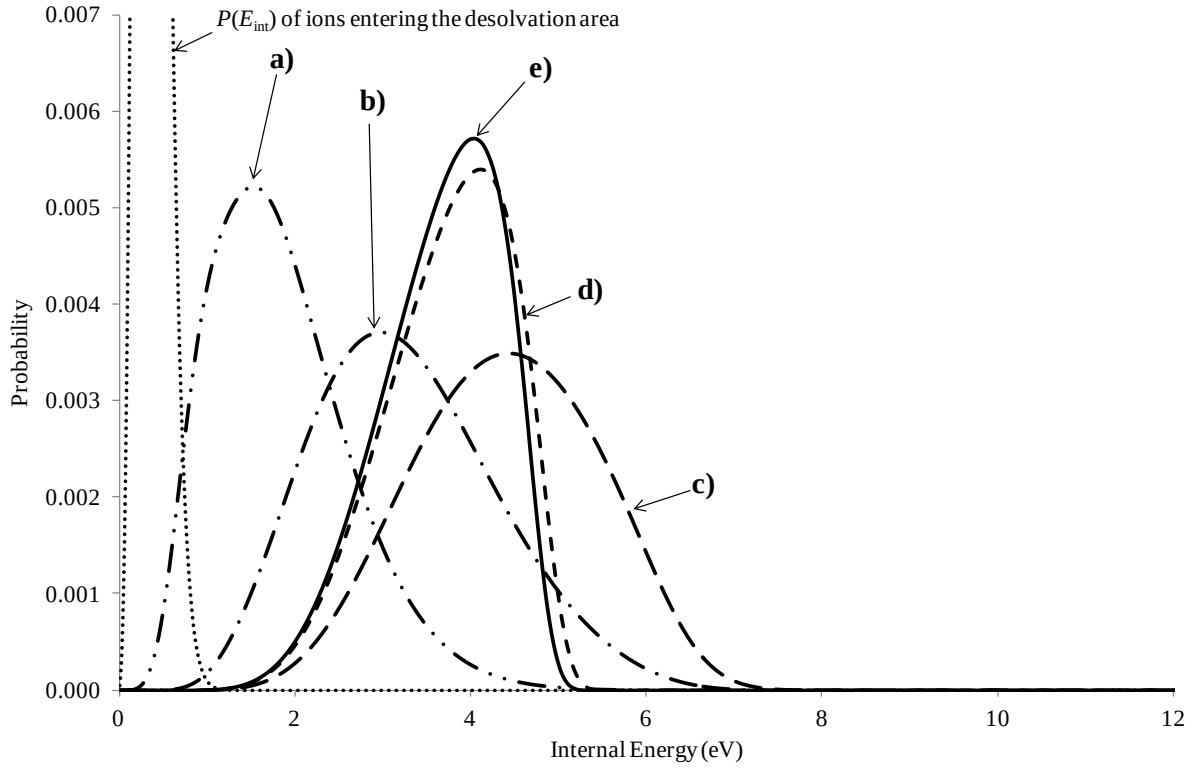

Figure 2: Internal energy distributions ($P(E_{int})$) of the pCH$_3$ cation calculated with a 35 Pa Pressure and a 8 eV initial kinetic energy (OR value = 40 V) at a distance of **a)** $4.33.10^{-3}$ m corresponding to the end of ion flight in the first third of the desolvation zone (—• •—), **b)** $8.67.10^{-3}$ m corresponding to the end of ion flight in the second third of the desolvation zone (—•—), **c)** $1.32.10^{-2}$ m corresponding to the end of the collision process when the ions leave the desolvation zone (— —), **d)** 0.223 m corresponding to the end of the ion guide (– –) and **e)** 0.423 m when the ions leave the quadrupole filter (——). The initial internal energy distribution of the ions at 353 K is magnified in the figure as dotted line (• •) in order to provide a better overview of the others $P(E_{int})$ related to the collision activation process.

The curve **a** in Figure 2 characterizes the $P(E_{int})$ of an ion population reaching the end of the first part of the collision region divided in three "slices". By referring to the initial thermal energy distribution at 353 K illustrated as a dotted line in Figure 2, it's appears that the shift of the initial internal energy distribution to higher values is accompanied by an enlargement of the curve and a tail in the relatively high values of E_{int}, *i.e.* typically until ~ 5 eV. In this first part of the desolvation area, the internal energy necessary for the observation of a fragmentation reaction in a time scale τ, is of 5.67 eV. The value of this appearance energetic threshold E_{thr} (see equation 2) can be evaluated from RRKM curves $\log\left[k^{i,j}(E_{int})\right]$ versus E_{int}

(see equation 3) as previously reported in literature.[35] This is done knowing the $k^{i,j}(E_{int})$ value from the inverse of the residence time τ of the ion expressed such as: $\tau = \left(1.018.10^{-4}\right) \cdot l \cdot \sqrt{\frac{m}{\Delta V}}$ (8) where m is the mass of the ion (in u), l is the length of the flight path (in m) and ΔV is the potential difference (in V).[31,54] In Figure 2, the tail to the high energies of the $P(E_{int})$ curve **a** do not reach the E_{thr} value calculated for a simulated pathway of $4.33.10^{-3}$ m. At this flight length, the dissociation process can be rule out and only the collision activation can be consider. By contrast, the competition between the activation and dissociation processes is illustrated through the curves **b** and **c** in Figure 2, these ones being related to the behaviour of ions leaving the second and the third part of the desolvation zone, respectively. In fact, as the ions leave the first part of the desolvation area, their flight length increases and the E_{thr} values necessary for fragmentation are then lowered to 5.37 and 5.19 eV, for the two other successive parts of the collision region. The dissociation reactions deplete the ion populations as the build-up of internal energy reaches the appearance energetic threshold E_{thr} (see equations 2 and 3). The occurrence of these two processes in parallel leads to truncated internal energy distributions as depicted in Figure 2 through the curves **b** and **c**.

Then, as the ions leave the collision region for entering into the designed ion guide, the activation process disappears. The evolution of the $P(E_{int})$ curves occurs only through a depletion of the high internal energy ion population as shown by the curves **d** and **e** in Figure 2. This suggests that in the case of this modelling, the internal energy distribution is redefined just by the lost of activated ions that dissociate into the ion guide (curve **d** in Figure 2). This truncated distribution that do not resemble to a thermal distribution, do not change notably as the ion leave the quadrupole filter (curve **e** in Figure 2).

The influence of the orifice voltage increasing on the internal energy build-up can be evidenced by evaluating the mean internal energy of untruncated distributions. For that, the occurrence of fragmentation reactions depleting the ion population must be rule for evaluating the internal energy distribution $P(E_{int})$ of the activated ions prior to their dissociation. This is done by setting a high value (typically 10 eV) of the critical energy of the fragmentation reaction of the substituted benzylpyridinium cations. By focussing on the case of the activated *p*-CH_3 cation, the internal energy distributions of these activated ions can be evaluated for the five values of initial kinetic energies ($E_{init,kin}$) related to the five experimental values of the Orifice. Theses internal energy distributions are depicted in Figure 3.

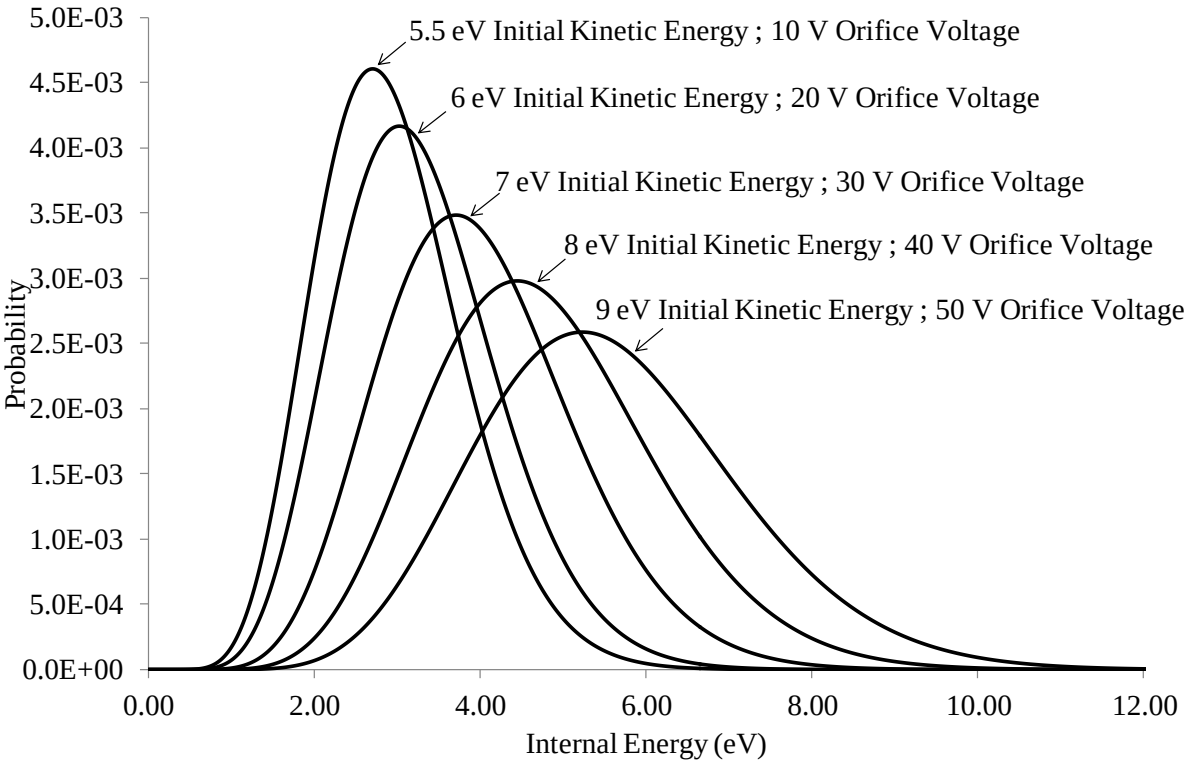

Figure 3: Internal energy distribution of the *p*-CH_3 cation prior to its decomposition, at the end of the collisional activation process modelised by the MassKinetics software for a 35 Pa Pressure and different initial kinetic energy ($E'_{\text{init.kin}}$) values of the ions entering to the collision area maintained under a potential difference so-called cone voltage value (see inserts in the Figure).

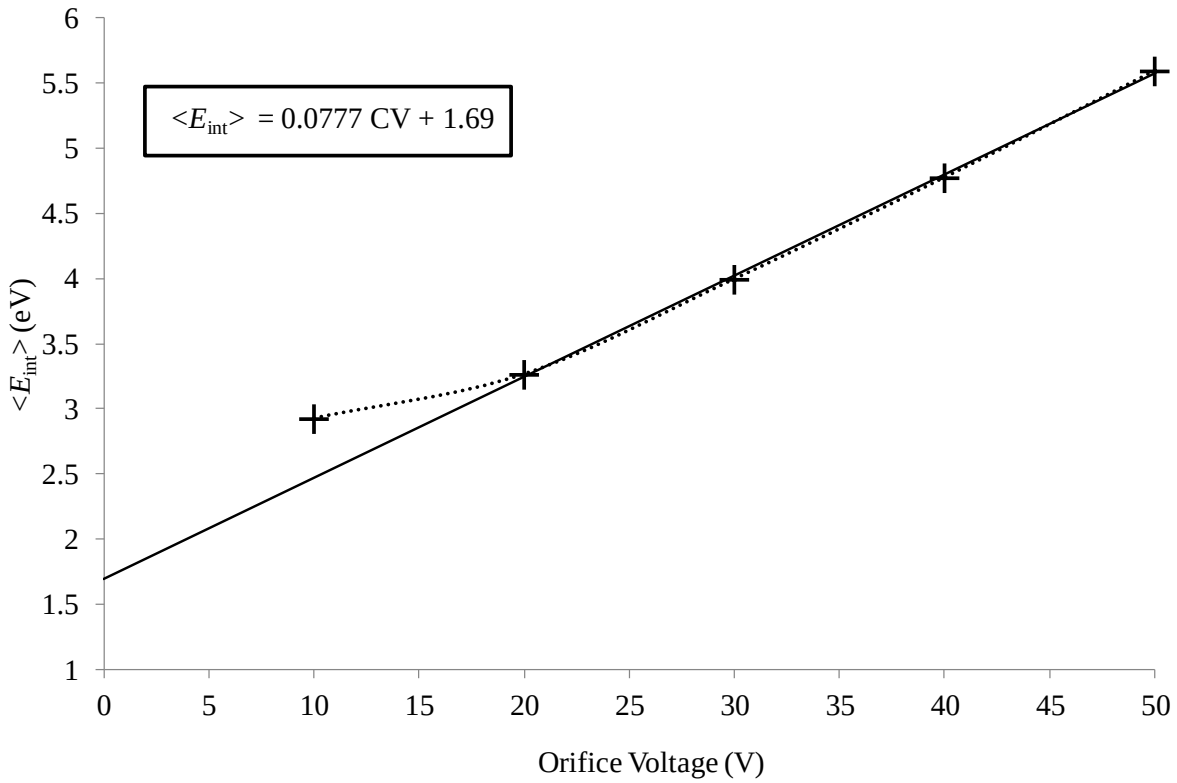

Figure 4: Mean internal energy of the pCH$_3$ cation $\langle E_{int} \rangle$ *vs.* Orifice Voltage. The average internal energies ($\langle E_{int} \rangle$) calculated from each curves are: $\langle E_{int} \rangle$ = 2.93 eV for $E'_{init.kin}$ = 5.5 eV ; $\langle E_{int} \rangle$ = 3.27 eV for $E'_{init.kin}$ = 6 eV ; $\langle E_{int} \rangle$ = 4.00 eV for $E'_{init.kin}$ = 7 eV ; $\langle E_{int} \rangle$ = 4.78 eV for $E'_{init.kin}$ = 8 eV and $\langle E_{int} \rangle$ = 5.60 eV for $E'_{init.kin}$ = 9 eV.

The average internal energies $\langle E_{int} \rangle$ expressed from the $P(E_{int})$ curves of Figure 3 can be plotted as a function of the voltage of the desolvation orifice (see Figure 4). The Figure 4 shows that from a 20 V value, the mean internal energy $\langle E_{int} \rangle$ increases linearly with the orifice voltage. This feature is in agreement with the data of literature.[37,40,42] Under a 20 V value, the mean internal energy tends to a constant value. As previously reported, this confirms that the 'ring lens' positioned close to the orifice (the desolation cone), do participate to ion activation, even at low cone voltages, since it's always kept at constant value.[31,32,40] From Figure 4, the linear extrapolation to zero cone voltage value leads to a mean internal energy $\langle E^{\circ}_{int} \rangle$ = 1.69 eV (see insert in Figure 4). This value is greater than the average internal energy $\langle E_{int} \rangle$ calculated for the source temperature, *i.e.* 0.37 eV for a thermal system at 353 K. This illustrates also the feasibility of hot ions formation in ESI due either to hot droplets involved in the release of the naked ion or to the kinetic energy of the "ejected" ions from the highly charged droplets in the context of the ion-evaporation model.[40]

The $P(E_{int})$ curves of Figure 3 show that the increasing in the colliding ion initial kinetic energy value associated with the orifice voltage value, leads to a shift the distributions to higher energy ranges. This is associated with a great increasing of the width of theses $P(E_{int})$. This trend is in agreement with the change of internal energy distribution with the temperature. These internal energy distributions calculated from the partially elastic multiple collision model shows also a significant high energy tail as thermal distributions for small molecules at relatively high temperatures. It means also that the colliding ions have reached a steady state of their internal energy distribution close to a Boltzmann distribution. If the $P(E_{int})$ curves of Figure 3 are "thermal-like" internal energy distributions, there is thermal energy distributions $P(E_{therm})$ such as the mean thermal energy $<E_{therm}>$ values are equal to the mean internal energy $<E_{int}>$ calculated from the curves of Figure 3. The $P(E_{therm})$ curves of the *p*-CH_3 cation can be obtained from the distribution of the thermal energy of the benzylpyridinium cation at different values of the temperature parameter, using the following expression:

$$P(E_{Therm}) = \frac{\rho(E_{int}) \cdot \exp\left(-E_{int} / k_B T\right)}{\int_0^{\infty} \rho(E_{int}) \cdot \exp\left(-E_{int} / k_B T\right)} \quad (9)$$

In equation 9, $\rho(E_{int})$ is the density of the vibrational state calculated from the frequency model, k_B the Boltzmann constant and T the term of temperature. Note that in this exact expression, the ergodicity principle leads to suppose that the excited states of all the vibration modes can be reach with the same probability. The Figure 5 regroups the $P(E_{therm})$ curves obtained from this calculation. The values of $<E_{int}>$ and the "characteristic" temperatures are plotted as a function of the orifice voltage (OR) variation in Figure 6.

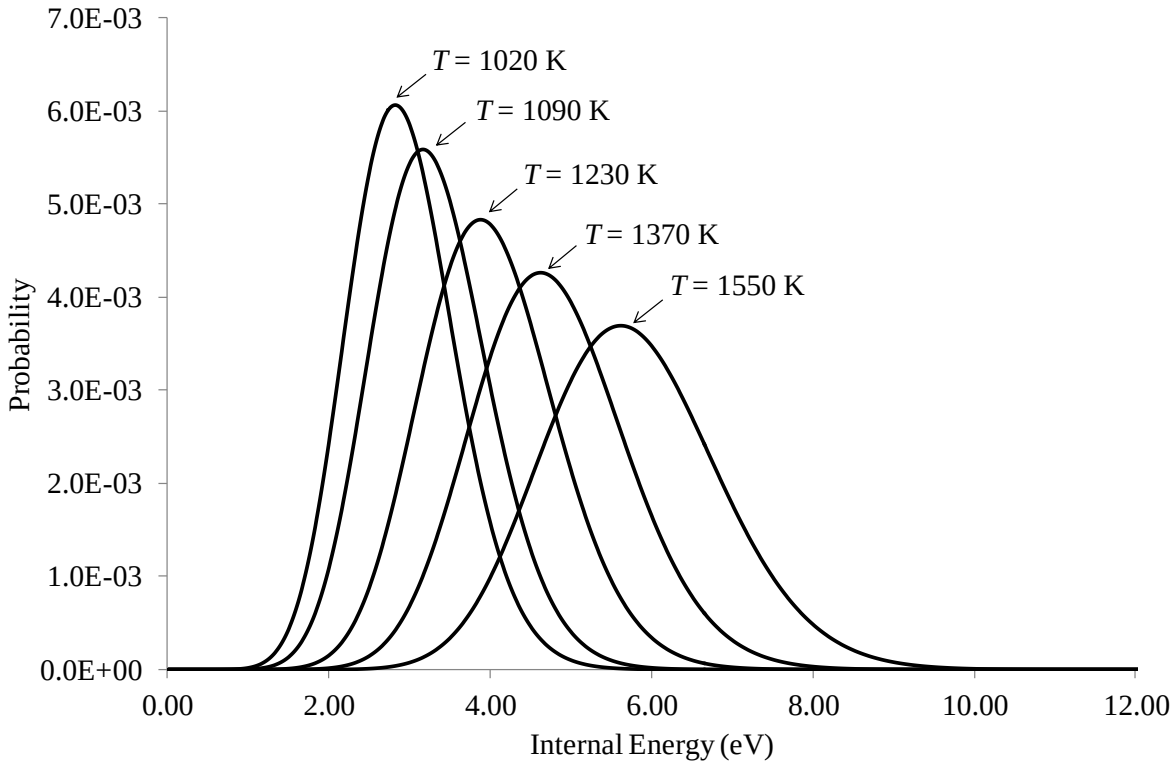

Figure 5: Thermal energy distribution of the paramethylbenzylpyridium cation (p-CH_3) at different 'characteristic' temperatures, where $<E_{int}>$ (from Figure 3) = $<E_{therm}>$ (from equation 9).

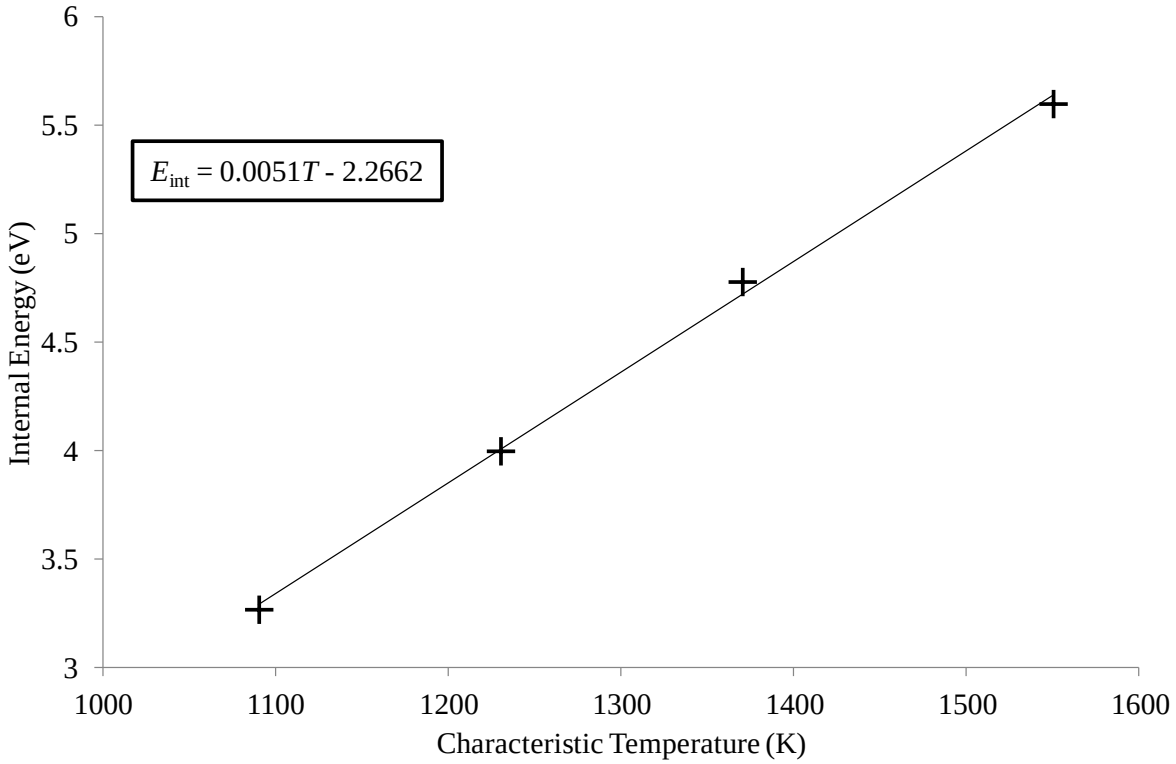

Figure 6: Plot of T_{char} *vs.* E_{int}.

The thermal energy distribution in Figure 5 resemble to the internal energy distribution of activated ion calculated from the collision model and depicted in Figure 3. This confirms that the model used for modelling the ion behaviour in the ESI interface account for a warm-up of colliding ion from 1090 to 1550 K. Another interesting result of this study is the linear correlation between $\langle E_{int} \rangle$ and T_{char} that is evidenced in Figure 6. The slop of the straight line can be interpreted through a small change in temperature allowing for writing the approximate form of an equation expressing an experimental parameter such as: $C_{Exp} = \left(\frac{\partial E_{int}}{\partial T} \right)_P = \left(\frac{\partial E_{Therm}}{\partial T} \right)_P$ = 0.0051 eV.K^{-1} (9) where C_{Exp} could be compared to the heat capacity of a system constituted by *N*-(4-methylbenzyl)pyridinium cations (*p*-CH_3) that does not dissociate. This experimental value can be compared to the value calculated from the derivative of the mean thermal energy (E_{therm}) as a function of *T*. Indeed if one considers the *p*-CH_3 cation having *s* = 78 oscillators and a set of frequencies ν_i obtained from its frequency file (see experimental section), the E_{therm} expression is:

$$E_{therm} = \sum_{i=1}^{s} \frac{h\nu_i}{\exp\left(h\nu_i / k_B T \right) - 1} \quad (10).$$

The derivative of the equation (10) allows for calculating the theoretical heat capacity parameter C_{Theo} from equation (11) where the different temperature values of Figure 6 leads to express C_{Theo} such as:

$$C_{Theo} = \frac{dE_{Therm}}{dT} = E_{Therm}^2 \cdot \frac{\sum_{i=1}^{s} \exp\left(h\nu_i / k_B T \right)}{k_B T^2} = 0.0028 \pm 7\% \quad (11).$$

This is a theoretical value that is relatively constant into the considered temperature range and is of the same magnitude order than the C_{Exp} value calculated from the Figure 6. This calorimetric parameter confirms that the ion activation into the desolvation area of the studied ESI source can be compared to a warm-up process.

CONCLUSION

1. Williams, D. H.; Howe, I. Principles of Organic Mass Spectrometry. McGraw-Hill Book Compagny (UK) Limited: London, 1972.

2. Vékey, K. Internal Energy Effects in Mass Spectrometry. *J. Mass Spectrom.* **1996**, *31*, 445-463.

3. McLafferty, F. W.; Tureček, F. Interpretation of Mass Spectra. Fourth Edition. University Science Books: Sausalito (California), 1993.

4. Whitehouse, C. M.; Dreyer, R. N.; Yamashita, M.; Fenn, J. B. Electrospray Interface for Liquid Chromatographs and Mass Spectrometers. *Anal. Chem.* **1985**, *57*, 675-679.

5. *Electrospray ionization mass spectrometry: Fundamentals, Instrumentation & Applications*, Cole RB (ed). John Wiley & Sons: New York, 1997; 107-136.

6. Gaskell, S. J. Electrospray : Principles and practice. *J. Mass Spectrom.* **1997**, *32*, 677-688.

7. Kebarle, P. A brief overview of the present status of the mechanisms involved in electropsray mass spectrometry. *J. Mass Spectrom.* **2000**, *35*, 804-817.

8. Cole, R. B. Some tenets pertaining to electrospray ionization mass spectrometry. *J. Mass Spectrom.* **2000**, *35*, 763-776.

9. Kebarle, P.; Verkerk, U. H. Electrospray: From ions in solution to ions in the gas-phase, what we know now? *Mass Spectrom*. Rev. **2009**, *28*, 870-897

10. Zhan, D.; Rosell, J.; Fenn, J. B. Solvation Studies of Electrospray Ions. Method and Early Results. *J. Am. Soc. Mass Spectrom.* 1998; **9**: 1241-1247.

11. Gabelica, V.; Lemaire, D.; Laprévote, O.; De Pauw, E. Kinetics of solvent addition on electrosprayed ions in an electrospray source and in a quadrupole ion trap. *Int. J. Mass Spectrom.* **2001**, *210/211*, 113-119.

12. Schlosser, G.; Takats, Z.; Vékey, K. Formation of solvated ions in the atmospheric interface of an electrospray ionization triplequadrupole mass spectrometer. *J. Mass Spectrom*. **2003**, *38*, 1245-1251.

13. Rondeau, D.; Perruchas, S.; Avarvari, N.; Batail, P.; Vékey, K. Electrospray ionization mass spectrometry of organic-inorganic materials: identification and gas-phase reactivity of functionalized octahedral rhenium(III) clusters. *J. Mass Spectrom*. **2005**, *40*, 60-65.

14. Fenn, J. B. Mass spectrometric implications of high-pressure ion sources. *Int. J. Mass Spectrom*. **2000**, *200*, 459-478.

15. Covey, T. R.; Thomson, B. A.; Schneider, B. B. Atmospheric pressure ion sources. *Mass Spectrom. Rev.* **2009**, *28*, 870-897.

16. Van Dongen, W. D.; van Wijk, J. I. T.; Green, B. N.; Heerma, W.; Haverkamp, J. Comparison between collision induced dissociation of electrosprayed protonated peptides in the up-front source region and in a low-energy collision cell. *Rapid Commun. Mass Spectrom.* **1999**, *13*,1712-1716.

17. Rogniaux, H.; Van Dorsselaer, A.; Barth, P.; Biellmann, J-F.; Barbanton, J.; van Zandt, M.; Chevrier, B.; Howard, E.; Mitschler, A.; Potier, N.; Urzhumtseva, L.; Moras, D.; Podjarny, A. Binding of aldose reductase inhibitors: correlation of crystallographic and mass spectrometric studies - A System for X-ray Crystallography and NMR. *J. Am. Soc. Mass Spectrom.* **1999**, *10*, 635-647.

18. Smith, R. D.; Barinaga, C. J. Internal energy effects in the collision-induced dissociation of large biopolymer molecular ions produced by electrospray ionization tandem mass spectrometry of cytochrome c. *Rapid Commun. Mass Spectrom*. **1990**, *4*, 54-57.

19. Gabelica, V.; De Pauw, E. Internal energy and fragmentation of ions produced in electrospray sources. *Mass Spectrom. Rev.* **2005**, *24*, 566-587.

20. De Pauw, E.; Pelzer, G.; Marien, J.; Natalis, P. Ion formation from Organic Solids. In *Spinger Proceedings in Physics*, A. Benningoven (Ed.). Spinger-Verlag: Heidelberg, **1986**, 103.

21. Collette, C.; De Pauw E. Calibration of the internal energy distribution of ions produced by electrospray. *Rapid Commun. Mass Spectrom.* **1998**, *12*, 165-70.

22. Williams, D. H.; Naylor, S. The internal energy distribution in Fast Atom Bombardment/Liquid Secondary Ion Mass Spectra. *J. Chem. Soc., Chem. Commun.* **1987**, 1408-1409.

23. Barylyuk, K. V.; Chingin, K.; Balabin, R. M.; Zenobi, R. Fragmentation of Benzylpyridinium "Thermometer" Ions and Its Effect on the Accuracy of Internal Energy Calibration. *J. Am. Soc. Mass Spectrom.* **2010**, 21, 172-177.

24. Zins, E. L. ; Pepe, C. ; Rondeau, D. ; Rochut, S.; Galland, N.; Tabet, J. C. Theoretical and experimental study of tropylium formation from substituted benzylpyridinium species. *J. Mass. Spectrom.* **2009**, *44*, 12–17.

25. Zins, E. L. ; Rondeau, D. ; Karoyan, P.; Fosse, C. ; Rochut, S.; Pepe, C. Investigations of the fragmentation pathways of benzylpyridinium ions under ESI/MS conditions. *J. Mass. Spectrom.* **2009**, *44*, 1668–1675.

26. Zins EL, Pepe C, Schröder D. Methylene-transfer reactions of benzylium/tropylium ions with neutral toluene studied by means of ion-trap mass spectrometry. *Faraday Discuss.* **2010**, *145*, 157-169.

27. Zins, E. L.; Pepe, C.; Schröder, D. Energy-dependent dissociation of benzylpyridinium ions in an ion-trap mass spectrometer. *J. Mass. Spectrom*. **2010**, *45*, 1253-1260.

28. Rosenstock, H. M.; Wallenstein, M. B.; Wahrhaftig, A. L.; Eyring, H. Absolute theory for isolated systems and the mass spectra of polyatomic molecules. *Proc. Nat. Acad. Sci. U.S.A.* **1952**, *38*, 667-678.

29. Marcus, R. A.; Rice, O. K. The kinetics of the recombination of methyl radicals and iodide atoms. *J. Phys. Colloid Chem.* **1951**, *55*, 894-908.

30. Marcus, R. A. Unimolecular dissociations and free radical recombination reactions. *J. Chem. Phys.* **1952**, *20*, 359-364.

31. Collette, C.; Drahos, L.; De Pauw, E.; Vékey, K. Comparison of the internal energy distributions of ions produced by different electrospray sources. *Rapid Commun. Mass Spectrom.* **1998**, *12*, 1673-1678

32. Drahos, L.; Heeren, R. M. A.; Collette, C.; De Pauw, E.; Vékey, K. Thermal energy distribution observed in electrospray ionization. *J. Mass Spectrom.* **1999**, *34*, 1373-1379.

33. Guo, X.; Duursma, M. C.; Kistemaker, P. G.; Nibbering, N. M. M,; Vékey, K.; Drahos, L.; Heeren, R. M. A. Manipulating internal energy of protonated biomolecules in electrospray ionization Fourier transform ion cyclotron resonance mass spectrometry. *J. Mass Spectrom.* **2003**, *38*, 597-606.

34. Gabelica,V. ; De Pauw, E.; Karas, M. Influence of the capillary temperature and the source pressure on the internal energy distribution of electrosprayed ions. *Int. J. Mass Spectrom*. **2004**, *231*, 189–195.

35. Rondeau, D.; Galland, N.; Zins, E. L.; Pepe, C.; Drahos, L.; Vékey, K. Non-Thermal Internal Energy Distribution of Ions Observed in an Electrospray Source Interfaced with a Sector Mass Spectrometer. *J. Mass Spectrom.* **2011**, *46*, 100-111.

36. Drahos, L.; Vékey, K. MassKinetics: A theoretical model of mass spectra incorporating physical processes, reaction kinetics and mathematical descriptions. *J. Mass Spectrom.* **2001**, *36*, 237-263

37. Naban-Maillet, J.; Lesage, D.; Bossée, A.; Gimbert, Y.; Sztáray, J.; Vékey, K.; Tabet, J. C. Internal energy distribution in electrospray ionization. *J. Mass Spectrom.* **2005**, *40*, 1-8.

38. Pak, A.; Lesage, D.; Gimbert, Y.; Vékey, K.; Tabet, J. C. Internal energy distribution of peptides in electrospray ionization: ESI and collision-induced dissociation spectra calculation. *J. Mass Spectrom.* **2008**, *43*, 447-455.

39. Drahos, L.; Vékey, K. Determination of the thermal energy and its distribution in peptides. *J. Am. Soc. Mass Spectrom.* **1999**, *10*, 323-328.

40. Takáts, Z.; Drahos, L.; Schlosser, G.; Vékey, K. Feasibility of formation of hot ions in electrospray. *Anal. Chem.* **2002**, *74*, 6427-6429.

41. Hoxha, A.; Collette, C.; De Pauw, E.; Leyh, B. Mechanism of Collisional Heating in Electrospray Mass Spectrometry: Ion Trajectory Calculations. *J. Phys. Chem. A* **2001**, *105*, 7326-7333.

42. Schneider, B. B.; Chen, D. D. Y. Collision-Induced Dissociation of Ions within the Orifice-Skimmer Region of an Electrospray Mass Spectrometer. *Anal. Chem.* **2000**, *72*, 791-799.

43. Baer, T.; Mayer, P. M. Statistical Rice-Ramsperger-Kassel-Marcus Quasiequilibrium Theory Calculations in Mass Spectrometry. *J. Am. Soc. Mass Spectrom.* **1997**, *8*, 103-115.

44. Robinson, P.J.; Holbrook, K. A. *Unimolecular Reactions*, Wiley: Chichester, 1972.

45. Baer, T.; Hase, W. L. *Unimolecular Reaction Dynamics*, Oxford University Press: Oxford, 1996.

46. Holmes, J. L.; Aubry, C.; Mayer, P. M. Proton Affinities of Primary Alkanols: An Appraisal of the Kinetic Method. *J. Phys. Chem. A* **1999**, *103*, 705-709.

47. Thomas, P. D.; Cooks, R. G.; Vékey, K.; Drahos, L.; Wesdemiotis, C. Comments on "Proton Affinities of Primary Alkanols: An Appraisal of the Kinetic Method". *J. Phys. Chem. A* **2000**, *104*, 1359-1361.

48. Dunbar, R. C. New approaches to ion thermochemistry via dissociation and association. In *Advances in Gas Phase Ion Chemistry*, Adams NG, Babcock LM (eds). JAI Press: Greenwich, **1996**, *2*, 87.

49. Gabelica, V.; Schultz, E.; Karas, M. Internal Energy build-up in matrix-assisted laser desorption/ionization. *J. Mass Spectrom.* **2004**, *39*, 579-593.

50. Oref, I.; Tardy, D. C. Energy Transfer in Highly Excited Large Polyatomic Molecules. *Chem. Rev*. **1990**, 1407-1445.

51. Muntean, F.; Armentrout, P. B. Guided ion beam study of collisioninduced dissociation dynamics: Integral and differential cross sections. *J. Chem. Phys.* 2001; **115**: 1213–1228.

52. Peltz, C.; Drahos, L.; Vekey, K. SORI excitation: Collisional and radiative processes. *J. Am. Soc. Mass. Spectrom.* **2007**, *18*, 2119–2126.

53. Sztáray, J.; Memboeuf, A.; Drahos, L.; Vékey, K. Leucine Enkephaline, a mass spectrometry standard. *Mass Spectrom. Rev.* **2011**, 30, 298– 320.

54. Vékey, K.; Somogyi, A.; Wysocki, V. Average Activation Energies of Low-energy Fragmentation Processes of Protonated Peptides Determined by a New Approach. *Rapid Commun. Mass Spectrom.* **1996**, *10*, 911-918.